

Observing gravitational wave polarizations with LISA-TAIJI network

Gang Wang^{1,*} and Wen-Biao Han^{1,2,†}

¹*Shanghai Astronomical Observatory, Chinese Academy of Sciences, Shanghai 200030, China*

²*School of Astronomy and Space Science, University of Chinese Academy of Sciences, Beijing 100049, China*

(Dated: February 28, 2025)

Two polarization modes of gravitational wave are derived from the general relativity which are plus and cross modes. However, the alternative theories of gravity can yield the gravitational wave with up to six polarizations. Searching for the polarizations beyond plus and cross is an important test of general relativity. In principle, one space-borne detector, like LISA, could measure the gravitational wave polarizations from a long time observation with its orbital motion. With the comparable sensitivities, the joint LISA and TAIJI missions will improve the observations on the polarization predictions of theories beyond general relativity. In this work, a class of parameterized post-Einsteinian waveform is employed to describe the alternative polarizations, and six parameterized post-Einsteinian parameters quantifying from general relativity waveform are examined by using the LISA-TAIJI network. Our results show that the measurements on amplitudes of alternative polarizations from joint LISA-TAIJI observation could be improved by more than 10 times compared to LISA single mission in an optimal scenario.

I. INTRODUCTION

From O1 to O3a of the Advanced LIGO and Virgo runs, About 50 gravitational wave (GW) events have been reported [1, 2]. The mergers of binary compact objects offer the unique chance to test general relativity (GR) in the extra strong and dynamical gravitational field [3–5]. During these tests, the polarization of GWs is an important issue. The general relativity (GR) predicts only two tensor polarizations: plus (+) and cross (×) modes. However, the metric theories of gravity may yield up to six polarizations which are two vector modes, two scalar modes, and the two transverse-traceless polarization modes in GR. For examples, scalar-tensor theories like as Brans-Dicke theory predict an extra scalar polarization (breathing, b) mode[6, 7]; Vector-tensor theories can excite vector modes (x, y modes); Einstein-aether theory [8] predicts the existence of five polarization modes; tensor-vector-scalar theories such as TeVeS[9], bimetric[10, 11] and stratified theories such as Lightman-Lee theory[12], predict the existence of all six polarization modes (+, ×, x, y, b, L), where L mode means longitudinal and is another scalar polarization mode.

In general, for the transient GW signals, at least three detectors are required to constrain additional modes[13]. Four detectors are necessary to constrain the vector modes, and in order to fully disentangle the polarization content of a transient signal, at least five detectors are needed to break all degeneracies[5, 13]. After the Advanced Virgo joined the GW observation network, the extra polarization modes have been tested with GW170814 [14]. The KAGRA in Japan has begun operating and will improve the measurement of polarizations in the near future [15–19].

The space-borne detectors including LISA [20], TAIJI [21], and TianQin [22] are planed to be launched around the 2030s targeting to detect the GW in the low frequency band. As a benefit of the periodical motions orbiting the Sun/Earth, the detectors can observe from (long-lasting) GW signals at different positions and orientations. And then one single mission, like LISA, could measure the polarizations independently, especially for the sources at optimal position and inclination. However, for the massive black hole binaries (MBHBs), the duration of the signal is about a few weeks and may not be enough to constrain the polarizations. The joint observation from LISA-TAIJI network may improve resolution of the measurements. With the comparable sensitivities of two missions, there will be lots of merits by LISA-TAIJI joint observations. Ruan *et al.* [23] and Wang *et al.* [24] demonstrated a significant improvement in sky localization capacities by LISA-TAIJI network. Omiya and Seto [25] and Orlando *et al.* [26] calculated the overlap reduction functions of the two missions and evaluated the impacts of the joint observations on the stochastic GW observation. Liu *et al.* [27] estimated the constraint on polarizations from single TAIJI observations.

In this paper, following our previous work in [24], by using the LISA-TAIJI network, we evaluate the capacity of observation for the polarization predictions beyond general relativity. A set of post-parameterized Einsteinian (ppE) waveform is employed to represent the GW signals of six potential polarization, and six ppE parameters are used to quantify the deviations of GW from GR. The Fisher information matrix algorithm is utilized to determine measurements on the six parameters from two MBHBs sources. The results show that the measurements on amplitudes of alternative polarizations from joint LISA-TAIJI observation could be improved by more than tenfold compared to LISA single mission in an optimal scenario.

This paper is organized as follows. In Sec. II, we introduce the model independent waveforms with GW and

* Gang Wang: gwang@shao.ac.cn, gwanggw@gmail.com

† Wen-Biao Han: Corresponding author: wuhan@shao.ac.cn

alternative polarization modes. In Sec. III, we specify the responding functions of the time-delay interferometry (TDI) to the polarizations, and evaluate the average sensitivities for the different polarization modes. The Fisher information matrix method utilized and the determinations on the ppE parameters are present in Sec. IV. And we recapitulate our conclusions in Sec. V. (We set $G = c = 1$ in this work).

II. PARAMETERIZED POST-EINSTEIN WAVEFORMS WITH ALL POLARIZATIONS

The GWs derived from GR have only two polarization modes h_+ and h_\times , the time-domain waveforms from a binary system with quadrupole approximation are

$$h_+ = -\frac{2\mu M}{Dr} \cos 2\Phi (1 + \cos^2 \iota), \quad (1)$$

$$h_\times = -\frac{4\mu M}{Dr} \sin 2\Phi \cos \iota, \quad (2)$$

where M the total mass, μ is the reduced mass $\frac{m_1 m_2}{m_1 + m_2}$, r the separation of two bodies, Φ the orbital phase, D is the luminosity distance, and ι inclination angle of the source with respect to the light-of-sight. The responded signal in a detector will to the GW be

$$h_{\text{GR}}(t) = F_+ h_+ + F_\times h_\times, \quad (3)$$

where F_+ and F_\times are antenna pattern functions of the detector to the two polarizations. On the other sides, the frequency evolution of a binary under PN approximation is a classical solved problem [28, 29], and the GW from GR in frequency-domain could be approximated as [30]

$$\tilde{h}_{\text{GR}}(f) = \left(\frac{5\pi}{96}\right)^{1/2} A_{\text{GR}} \frac{\mathcal{M}^2}{D} (\pi \mathcal{M} f)^{-7/6} e^{-i\Psi_{\text{GR}}}, \quad (4)$$

where \mathcal{M} is the chirp mass of the binary $(m_1 m_2)^{3/5} / (m_1 + m_2)^{1/5}$, A_{GR} is the responding amplitude of polarization modes (+, \times) from a detector

$$A_{\text{GR}} = -F_+(1 + \cos^2 \iota) - 2iF_\times \cos \iota. \quad (5)$$

In general, GW metric perturbations at a given space-time point can be expressed as

$$h_{ij}(t, \hat{\Omega}) = h_a(t) e_{ij}^a(\hat{\Omega}), \quad (6)$$

where $\hat{\Omega}$ is the sky direction of a GW source. In metric theories of gravity, there are up to six possible polarization modes because the polarization tensors $e_{ij}^a(\hat{\Omega})$ could have maximum six combinations which are defined as

$$e_{ab}^+ = \hat{e}_x \otimes \hat{e}_x - \hat{e}_y \otimes \hat{e}_y, \quad (7)$$

$$e_{ab}^\times = \hat{e}_x \otimes \hat{e}_y + \hat{e}_y \otimes \hat{e}_x, \quad (8)$$

$$e_{ab}^x = \hat{e}_x \otimes \hat{e}_z + \hat{e}_z \otimes \hat{e}_x, \quad (9)$$

$$e_{ab}^y = \hat{e}_y \otimes \hat{e}_z + \hat{e}_z \otimes \hat{e}_y, \quad (10)$$

$$e_{ab}^b = \hat{e}_x \otimes \hat{e}_x + \hat{e}_y \otimes \hat{e}_y, \quad (11)$$

$$e_{ab}^L = \sqrt{2} \hat{e}_z \otimes \hat{e}_z, \quad (12)$$

where the set of orthonormal unit vectors $\{\hat{e}_x, \hat{e}_y, \hat{e}_z\}$ is GW basis, i.e., $\hat{e}_z = -\hat{\Omega}$ is a unit vector in the direction of propagation of the GW and $\hat{e}_z = \hat{e}_x \times \hat{e}_y$. Then in Eq. (6), $a = +, \times, x, y, b, L$ are the polarization indices and corresponding to the two tensor modes (h_+, h_\times), two vector modes (h_x, h_y) and two scalar modes (breathing h_b and longitudinal h_L).

By assuming all six polarization modes exist, an observed GW signal in a detector can be written as

$$h(t) = F_+ h_+ + F_\times h_\times + F_x h_x + F_y h_y + F_b h_b + F_L h_L. \quad (13)$$

Similar to Eq. (3), the F_x, F_y, F_b , and F_L are the response functions of the detector to the extra polarization modes beyond the GR. However, the h_x, h_y, h_b and h_L are the GW waveform for the corresponding polarizations, and they are derived in a different forms from various theories. Also not all the polarization modes appears in different theories. For instance, the Brans-Dicke theory (a scalar-tensor theory) only predicts one more mode h_b . We select GW waveforms derived from Rosen's theory [10, 11] to illustrate the extra four polarizations,

$$h_b = \frac{2\mu}{D} \left[\frac{m}{r} \sin^2 \iota \sin^2 \Phi + \frac{m}{r} - \frac{4}{3} \left(\frac{m}{r} \right)^{1/2} \mathcal{G} \sin \iota \cos \Phi \right], \quad (14)$$

$$h_L = \frac{4\mu}{D} \left[\frac{m}{r} \sin^2 \iota \sin^2 \Phi - \frac{m}{r} - \frac{2}{3} \left(\frac{m}{r} \right)^{1/2} \mathcal{G} \sin \iota \cos \Phi \right], \quad (15)$$

$$h_x = \frac{4\mu}{D} \left[\frac{m}{r} \sin^2 \Phi \sin \iota \cos \iota - \frac{2}{3} \left(\frac{m}{r} \right)^{1/2} \mathcal{G} \cos \Phi \sin \iota \right], \quad (16)$$

$$h_y = \frac{4\mu}{D} \left[-\frac{m}{r} \cos \Phi \sin \Phi \sin \iota - \frac{2}{3} \left(\frac{m}{r} \right)^{1/2} \mathcal{G} \sin \Phi \right], \quad (17)$$

where \mathcal{G} is the difference in the self-gravitational binding energy per unit mass of the binary components, and it becomes to zero in GR. And the waveforms in frequency-domain have different formulas for different theories not only due to the time-domain waveforms but also due to varied radiation reactions. A general framework which can incorporate the possible alternative theories of gravity will be convenient to test the potential polarizations beyond the GR.

To test the GR in the post-Newtonian limits, the parameterized post-Newtonian (ppN) formalism was developed in the 1970s [31–33]. The ppN formalism provided a good approach on tests of gravity theories in the solar system, binary pulsars, motion of objects around supermassive black hole, and etc [7]. To test the alternative theories of gravity beyond the GR, by adopting the similar strategy like ppN, Yunes and Pretorius [34] developed a parameterized post-Einsteinian (ppE) formalism to incorporate the alternative theories beyond GR. Chatziioannou *et al.* [13] extended a model-independent

framework to including the complete polarization content. The ppE approach provides a approach for testing GR through the GW observations.

The standard ppE waveform in frequency domain can be generally expressed as

$$\tilde{h}(f) = \tilde{h}_{\text{GR}}(f)[1 + \alpha u^a]e^{i\beta u^b}, \quad (18)$$

where (α, a) are ppE parameters on the amplitude modification, and (β, b) are parameters on phase correction. $u = \pi \mathcal{M}f$ when the dominant GW mode is considered. The waveform will return to the PN waveform described in GR $\tilde{h}_{\text{GR}}(f)$ as when the ppE parameters go to zero.

When full six possible polarization modes are considered, by taking the waveform from harmonic $l = 2$, a model-independent ppE framework from [13] are described as

$$\begin{aligned} \tilde{h}_{\text{ppE}}(f) = & \tilde{h}_{\text{GR}} \left(1 + c\beta u_2^{b+5} \right) e^{2i\beta u_2^b} + [\alpha_b F_b \sin^2 \iota \\ & + \alpha_L F_L \sin^2 \iota + \alpha_x F_x \sin 2\iota + \alpha_y F_y \sin \iota] \\ & \times \frac{\mathcal{M}^2}{D} u_2^{-7/2} e^{-i\Psi_{\text{GR}}^{(2)}} e^{2i\beta u_2^b}, \end{aligned} \quad (19)$$

where $u_2 \equiv (\pi \mathcal{M}f)^{1/3}$ as defined in this case, β and b are the free ppE parameters, c is a coefficient decided by b . α_b , α_L , α_x , and α_y are the parameters related to the breathing, longitudinal and vector polarization x and y modes, respectively. $F_{b,L,x,y}$ are the response functions of one GW detector to each corresponding polarization mode. c is defined as follow to incorporate the conservative and dissipative corrections as defined by Eq. (169) in [13],

$$c = -\frac{16}{15} \frac{b(3-b)(b^2 + 7b + 4)}{b^2 + 8b + 9}. \quad (20)$$

The relation between b and c means that the modification on the GW phase will definitely influences on the amplitude as analyzed in [13]. The GW approximation in this work is based on the Eq. (19), and the antenna pattern functions for polarization mode p, F_p for a LISA-like detectors will be specified in the next section.

III. GW RESPONSE IN TDI

A. The LISA and TAIJI orbital configuration

The updated LISA mission proposed a 2.5×10^6 km arm length and trails the Earth by around 20° [20]. The formation plane of the three S/C would has 60° inclination angle with respect to the ecliptic plane as shown in Fig. 1. The TAIJI mission proposed a LISA-like formation which 3×10^6 km arm length [21]. The triangle constellation will in front of the Earth by around 20° as shown in Fig. 1.

With a separation of $\sim 1 \times 10^8$ km, and the joint LISA-TAIJI observation from the long baseline will bring merits for GW detections. In our previous work [24], we

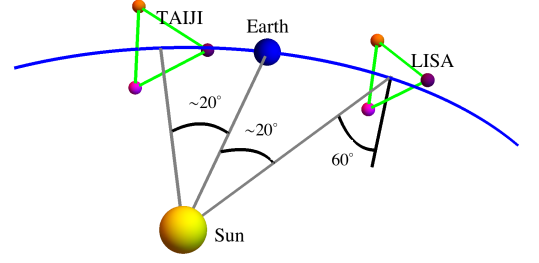


FIG. 1. The diagram of LISA and TAIJI mission orbital configurations.

evaluated the sky localization improvement of the joint observation on the supermassive black hole binaries. By employing the numerical mission orbit in [24, 35], we will explore the detectability of the joint network to the alternative GW polarization modes beyond the GR.

B. Michelson and optimal TDI channels

The optimal channels of the first-generation Michelson TDI channel are employed to perform the detectability of the LISA/TAIJI mission. The Michelson X channel spacecraft (S/C) layout-time delay diagram is shown in Fig. 2 as generated in [36]. Following the diagram, the

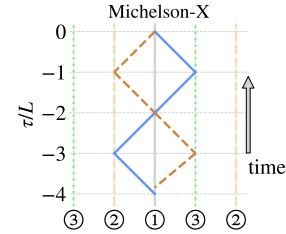


FIG. 2. The S/C layout-time delay diagrams for Michelson X channels as generated in [36].

expression of measurements in the X channel will be [37].

$$\begin{aligned} X = & [\mathcal{D}_{31}\mathcal{D}_{13}\mathcal{D}_{21}\eta_{12} + \mathcal{D}_{31}\mathcal{D}_{13}\eta_{21} + \mathcal{D}_{31}\eta_{13} + \eta_{31}] \\ & - [\eta_{21} + \mathcal{D}_{21}\eta_{12} + \mathcal{D}_{21}\mathcal{D}_{12}\eta_{31} + \mathcal{D}_{21}\mathcal{D}_{12}\mathcal{D}_{31}\eta_{13}] \end{aligned} \quad (21)$$

where \mathcal{D}_{ij} is a time-delay operator, $\mathcal{D}_{ij}\eta(t) = \eta(t - L_{ij})$. The η_{ji} are the combined observables from S/Cj to S/Ci which are defined as [38–40], and the specific expressions for this work are defined by Eq. (2) in [36].

A group of optimal TDI channels, (A, E, and T), can be generated from linear combinations of the three Michel-

son channels (X, Y, and Z) as following [41, 42],

$$A = \frac{Z - X}{\sqrt{2}}, \quad E = \frac{X - 2Y + Z}{\sqrt{6}}, \quad T = \frac{X + Y + Z}{\sqrt{3}}. \quad (22)$$

The Y and Z channels are obtained from cyclical permutation of the S/C indexes. The joint three optimal channels would represent the ultimate detectability of a LISA-like space mission. Therefore, the joint optimal channels are employed to study the capability of the LISA and TAIJI mission to the GW signals.

C. Response formulation of TDI channel

The final GW response of a TDI channel is combined from the response in each single link. The response to a

GW + and \times polarizations in a single link Doppler measurement has been formulated in [43, 44], and specific formulas were described in Vallisneri and Galley [37], Vallisneri *et al.* [42]. To investigate the response of TDI to the alternative polarizations beyond the GR, we extend the formulas as follows.

For a GW source locating at ecliptic longitude λ and latitude θ with respect to the solar-system barycentric coordinates, the GW propagation vector will be

$$\hat{k} = -(\cos \lambda \cos \theta, \sin \lambda \cos \theta, \sin \theta). \quad (23)$$

The + or \times polarization tensors of the GW signal, as well as the (potential) alternative polarization tensor, scalar breathing (b), scalar longitudinal (L), vector x and y, combining with the factors from inclination angle ι of the source are

$$\begin{aligned} e_+ &\equiv \mathcal{O}_1 \cdot \begin{pmatrix} 1 & 0 & 0 \\ 0 & -1 & 0 \\ 0 & 0 & 0 \end{pmatrix} \cdot \mathcal{O}_1^T \times \frac{1 + \cos^2 \iota}{2}, & e_\times &\equiv \mathcal{O}_1 \cdot \begin{pmatrix} 0 & 1 & 0 \\ 1 & 0 & 0 \\ 0 & 0 & 0 \end{pmatrix} \cdot \mathcal{O}_1^T \times i(-\cos \iota), \\ e_b &\equiv \mathcal{O}_1 \cdot \begin{pmatrix} 1 & 0 & 0 \\ 0 & 1 & 0 \\ 0 & 0 & 0 \end{pmatrix} \cdot \mathcal{O}_1^T \times \sin^2 \iota, & e_L &\equiv \mathcal{O}_1 \cdot \begin{pmatrix} 0 & 0 & 0 \\ 0 & 0 & 0 \\ 0 & 0 & 1 \end{pmatrix} \cdot \mathcal{O}_1^T \times \sin^2 \iota, \\ e_x &\equiv \mathcal{O}_1 \cdot \begin{pmatrix} 0 & 0 & 1 \\ 0 & 0 & 0 \\ 1 & 0 & 0 \end{pmatrix} \cdot \mathcal{O}_1^T \times \sin \iota \cos \iota, & e_y &\equiv \mathcal{O}_1 \cdot \begin{pmatrix} 0 & 0 & 0 \\ 0 & 0 & 1 \\ 0 & 1 & 0 \end{pmatrix} \cdot \mathcal{O}_1^T \times i \sin \iota, \end{aligned} \quad (24)$$

with

$$\mathcal{O}_1 = \begin{pmatrix} \sin \lambda \cos \psi - \cos \lambda \sin \theta \sin \psi & -\sin \lambda \sin \psi - \cos \lambda \sin \theta \cos \psi & -\cos \lambda \cos \theta \\ -\cos \lambda \cos \psi - \sin \lambda \sin \theta \sin \psi & \cos \lambda \sin \psi - \sin \lambda \sin \theta \cos \psi & -\sin \lambda \cos \theta \\ \cos \theta \sin \psi & \cos \theta \cos \psi & -\sin \theta \end{pmatrix}, \quad (25)$$

where ψ is the polarization angle. The response to the GW polarization p in the link from S/Ci to j will be

$$y_{p,ij}^h(f) = \frac{\hat{n}_{ij} \cdot \mathbf{e}_p \cdot \hat{n}_{ij}}{2(1 - \hat{n}_{ij} \cdot \hat{k})} \times \left[\exp(2\pi i f (L_{ij} + \hat{k} \cdot \mathbf{p}_i)) - \exp(2\pi i f \hat{k} \cdot \mathbf{p}_j) \right], \quad (26)$$

where \hat{n}_{ij} is the unit vector from S/Ci to j, L_{ij} is the arm length from S/Ci to j, \mathbf{p}_i is the position of the S/Ci in the SSB coordinates.

The response of a TDI combination for a specific polarization p in the frequency domain will be simplified by summing up the responses in the time shift single links. For instance, the response in the X channel could be described by

$$\begin{aligned} F_{X,p}(f) &= (-\Delta_{21} + \Delta_{21}\Delta_{13}\Delta_{31})y_{p,12}^h \\ &\quad + (-1 + \Delta_{13}\Delta_{31})y_{p,21}^h \\ &\quad + (\Delta_{31} - \Delta_{31}\Delta_{12}\Delta_{21})y_{p,13}^h \\ &\quad + (1 - \Delta_{12}\Delta_{21})y_{p,31}^h, \end{aligned} \quad (27)$$

where $\Delta_{ij} = \exp(2\pi i f L_{ij})$. The GW responses in the

optimal A, E, and T channels are obtained by applying Eq. (22) straightforwardly. One polarization of GW waveform in a TDI channel could be expressed as $\tilde{h}_{\text{TDI},p} = F_{\text{TDI},p} \tilde{h}$ as it will be shown in Fig. 4, where the \tilde{h} is the *intrinsic* GW waveform in the frequency domain. By using Eq. 19, The alternative GW waveform with six polarizations in one TDI channels could be modified as [45]

$$\begin{aligned} \tilde{h}_{\text{ppE,TDI}}(f) &= [(F_+ + F_\times)(1 + c\beta u_2^{b+5}) + \alpha_b F_b + \alpha_L F_L \\ &\quad + \alpha_x F_x + \alpha_y F_y] \tilde{h}_{\text{GR}} e^{2i\beta u_2^b}, \end{aligned} \quad (28)$$

where \tilde{h}_{GR} is the intrinsic GW waveform from GR which described by the approximant IMRPhenomPv2 [46] in

our calculations. The $\beta, b, \alpha_b, \alpha_L, \alpha_x$ and α_y are the six ppE parameters to be determined.

D. The average sensitivities of LISA to the polarizations

Considering the various response in TDI channels, we evaluate the average sensitivities of the LISA and LISA-TAIJI network to the six polarization modes at first. Following the method we used in Wang *et al.* [36], 10^5 sources are simulated randomly which are located over the sky and polarization at each frequency. The response of one TDI channels to a polarization mode is calculated by using the Eq. (22)-(27) with an optimal inclination, (for instance, inclination $\iota = 0$ yields the maximum amplitude for tensor polarization, and $\iota = \pi/2$ yields the strongest GW for scalar polarizations). The median responses of joint A+E+T channels over sky and polarization angle are chosen to represent the average capacity of one mission to a specific GW polarization mode. And the response of LISA and TAIJI to a source are calculated simultaneously.

The acceleration noise and optical path noise are considered to evaluate the sensitivity of LISA/TAIJI. The noise budgets are from the updated upper limit of their noise requirements [20, 47]. The acceleration noise S_{acc} requirements are assumed to be the same for both LISA and TAIJI,

$$S_{\text{acc}}^{1/2} = 3 \times 10^{-15} \frac{\text{m/s}^2}{\sqrt{\text{Hz}}} \sqrt{1 + \left(\frac{0.4\text{mHz}}{f}\right)^2} \sqrt{1 + \left(\frac{f}{8\text{mHz}}\right)^4}. \quad (29)$$

And the optical path noises S_{op} requirement for two missions are slightly different which are

$$S_{\text{op,LISA}}^{1/2} = 10 \times 10^{-12} \frac{\text{m}}{\sqrt{\text{Hz}}} \sqrt{1 + \left(\frac{2\text{mHz}}{f}\right)^4}, \quad (30)$$

$$S_{\text{op,TAIJI}}^{1/2} = 8 \times 10^{-12} \frac{\text{m}}{\sqrt{\text{Hz}}} \sqrt{1 + \left(\frac{2\text{mHz}}{f}\right)^4}.$$

The combined noise PSDs of the TDI channels are calculated by implementing the algorithm in [36, 48].

The average sensitivities of the LISA's A+E+T channel and joint LISA-TAIJI network to a polarization mode p are obtained by,

$$S_{\text{LISA,p}} = \left(\sum_{\text{A,E,T}} \frac{|F_{\text{TDI,p}}|^2}{S_{\text{n,TDI}}} \right)^{-1}, \quad (31)$$

$$S_{\text{joint,p}} = \left(\sum_{\text{LISA}} \sum_{\text{A,E,T}} \frac{|F_{\text{TDI,p}}|^2}{S_{\text{n,TDI}}} \right)^{-1}.$$

The average sensitivities of the LISA mission for different polarization modes are shown in the upper panel of

Fig. 3. The upper plot of the upper panel shows the increase of joint A+E+T sensitivity compared to the fiducial Michelson X channel. As we expatiated in Wang *et al.* [48], the joint A+E+T channels will improve the sensitivity by a factor of $\sqrt{2}$ to 2 times than X single channel. The joint LISA-TAIJI observation can further improve the sensitivity of LISA by a factor of $\geq \sqrt{2}$ as shown in the lower panel of Fig. 3. We can also notice that the sensitivity for vector mode and the longitudinal mode not quickly decline as the tensor mode, and this should be due to the higher response at high frequency band in the TDI for these polarization modes as discussed in [49, 50].

The sensitivities for alternative polarizations in Fig. 3 are calculated by assuming the ppE parameter $\alpha_i = 1$ in Eq. (28) and an optimal inclination ι in Eq. (24). The sensitivities could be scaled by the tuned factors.

IV. CONSTRAIN PPE PARAMETERS FROM SMBH BINARY

A. Source selections

Following our previous work [24], we choose the SMBH binaries with mass ratio $q = 1/3$ at redshift $z = 2$ to examine the detectability of the LISA-TAIJI network and compare the results to a single LISA mission. Two masses setups are employed which are source1 ($m_1 = 10^5 M_\odot, m_2 = 3.3 \times 10^4 M_\odot$) and source2 ($m_1 = 10^6 M_\odot, m_2 = 3.3 \times 10^5 M_\odot$). Another motivation for this selection is that these two sources could be well sky localized by the two detector network as we studied in [24]. Therefore, an optimistic scenario would be assumed that the source location (direction and distance) could be determined by multi-messenger observation, and the known source location may improve the analysis results.

The redshifted GW amplitudes of two sources in the selected TDI channels and the ASDs of the channels are shown in Fig. 4, and the amplitudes incorporate the response function of the TDI channels $2\sqrt{f}|\tilde{h}_{\text{GR}}*F_{\text{TDI,p}}|$ for the specific source parameters ($\theta = \pi/10, \iota = 0.55, \psi = \pi/3$) through the frequency band in the last 30 days coalescing. The ASDs of the TDI channels are the noise level from the acceleration and optical-path noises. The ASDs of A and E channels are identical, while the amplitudes of GW signals in their channels are different. As we previously studied in [36, 48], the location around the ecliptic latitude $\theta = 18^\circ$ is an optimal choice for the average response, and the longitude of sources is coordinated with the positions of the LISA and TAIJI to have an optimal response. The inclination of the sources is one of the key factors which relates to the cadence of the different polarization amplitudes. By presuming the polarization modes beyond GR are much less significant than $+/ \times$ polarizations from GW, the inclination angle is set to be $\iota = 0.55$ which is close to the favored angle of the detections as shown in the upper plot of Fig. 5 [51].

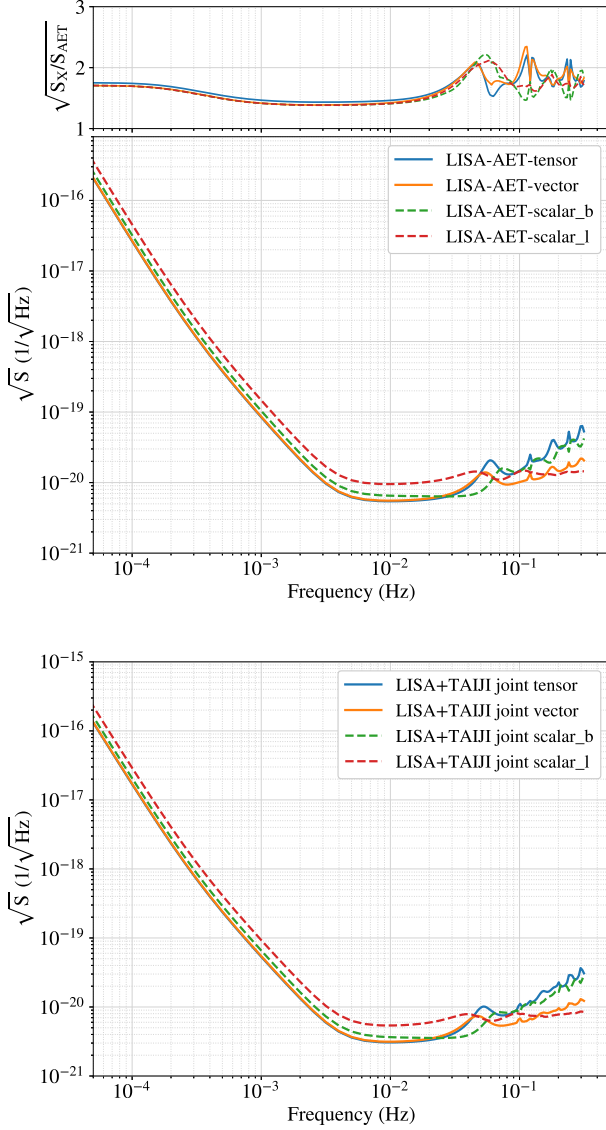


FIG. 3. The average sensitivities of LISA mission (upper panel) and joint LISA-TAIJI network (lower panel) to the different polarization modes at the optimal inclination angles. The upper plot of the upper panel shows the joint LISA A+E+T channel would improve the sensitivity by a factor of $\sqrt{2}$ to 2 compared to its fiducial Michelson X channel. The lower panel shows the joint LISA-TAIJI network can improve the sensitivities by a factor of $\geq \sqrt{2}$ than the single LISA mission.

And we will also perform the investigations varying with the inclination in Section IV C. The polarization angle is set to be $\psi = \pi/3$.

For the source1 ($m_1 = 10^5 M_\odot, q = 1/3$), the GW frequency evolution during the last 30 days to merger will change from 0.35 mHz to 40 mHz, and the corresponding $u_2^3 = \pi \mathcal{M} f$ value changes from [0.0008, 0.09]. And the GW frequency from the binary ($m_1 = 10^6 M_\odot, q = 1/3$) will start from 0.08 mHz to 4 mHz, and the range of u_2^3

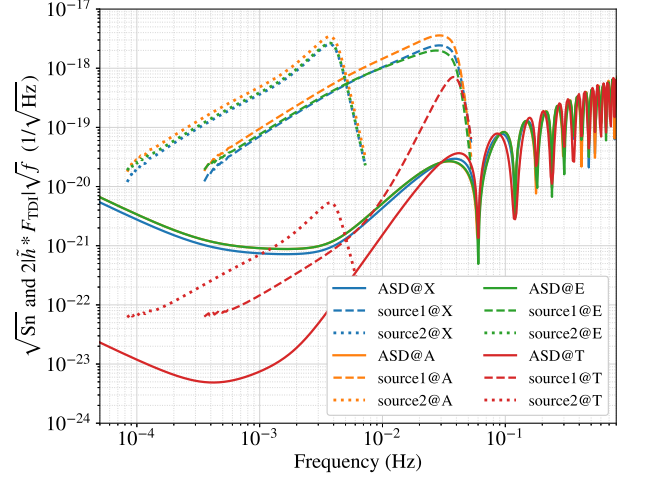


FIG. 4. The redshifted GW amplitudes $2\sqrt{f}|\tilde{h}_{\text{GR}} * F_{\text{TDI},p}|$ of the selected sources and ASDs in the TDI channels. The GW amplitudes include the TDI response function $F_{\text{TDI},p}$ for the sources with geometric angles ($\theta = \pi/10, \iota = 0.55, \psi = \pi/3$). The ASDs of the TDI noises include the acceleration noises and optical path noises. The source1@TDI indicates GW amplitude of the source1 ($m_1 = 10^5 M_\odot, q = 1/3, z = 2$) in the TDI channels, and source2@TDI indicates the source2 ($m_1 = 10^6 M_\odot, q = 1/3, z = 2$).

is [0.002, 0.09]. As estimated in Cornish *et al.* [52], the bounds limits of β at given b is expected to be inversed proportional to the SNR and the range of u_2^b .

B. Fisher information method

The Fisher Information Matrix (FIM) is applied in this investigation to determine the uncertainty of parameter estimation from GW observation as used in [24, 53–56, and references therein]. The FIM from the single LISA mission is obtained by summing up the three optimal channels (A, E, and T), and the joint FIM of the LISA-TAIJI network is achieved by summing up the FIM from each mission,

$$\Gamma_{ij} = \sum_{\text{LISA}} \sum_{\text{A,E,T}}^{\text{TAIJI}} \left(\frac{\partial \tilde{h}_{\text{ppE,TDI}}}{\partial \xi_i} \middle| \frac{\partial \tilde{h}_{\text{ppE,TDI}}}{\partial \xi_j} \right), \quad (32)$$

with

$$(g|h)_{\text{TDI}} = 4\text{Re} \int_0^\infty \frac{g^*(f)h(f)}{S_{\text{TDI}}(f)} df, \quad (33)$$

where $\tilde{h}_{\text{ppE,TDI}}$ is the frequency domain GW waveform with all polarization modes as described by Eq. 28, ξ_i is the i -th parameter to be determined, and $S_{\text{TDI}}(f)$ is the noise PSD of one TDI channel from LISA or TAIJI.

In this investigation, 15 parameters are considered to describe the GW signal from a binary system which

are ecliptic longitude and latitude (λ, θ) , polarization angle ψ , inclination ι , luminosity distance D , the coalescence time and phase (ϕ_t, ϕ_c) , the total mass of binary M and mass ratio q , and the six ppE parameters $(\beta, b, \alpha_b, \alpha_L, \alpha_x, \alpha_y)$. Two scenarios are considered to implement the FIM calculations, the first one is the location of the source is unknown and the FIM is calculated for full 15 parameters, the second case is the location of GW source is known from other associated observation and FIM is calculated for 12 parameters excluding the three parameters, (λ, θ, D) .

The variance-covariance matrix of the parameters could be obtained by

$$\langle \Delta \xi_i \Delta \xi_j \rangle = (\Gamma^{-1})_{ij} + \mathcal{O}(\rho^{-1}) \quad (34)$$

The standard deviations σ_i and correlation coefficients σ_{ij} of the parameters for the high SNR $\rho \gg 1$ will be

$$\begin{aligned} \sigma_i &\simeq \sqrt{(\Gamma^{-1})_{ii}}, \\ \sigma_{ij} &= \frac{\text{cov}(\xi_i, \xi_j)}{\sigma_i \sigma_j} \simeq \frac{(\Gamma^{-1})_{ij}}{\sigma_i \sigma_j}. \end{aligned} \quad (35)$$

We focus on the ppE parameters determinations from LISA and the improvements from LISA-TAIJI joint observations in this work.

C. Results with varying inclination

We examine the detectability of the ppE parameter varying with the inclination of sources in this subsection. The amplitude of a GW signal is modulated with the inclination ι of the binary as we can read from Eq. (24). With only considering the two GW polarizations from GR, the distribution of inclination ι from detections is expected to be [51]

$$p_{\text{tensor}}(\iota) \propto (1 + 6 \cos^2 \iota + \cos^4 \iota)^{3/2} \sin \iota. \quad (36)$$

The normalized distribution is shown by the blue curve in the upper plot of Fig. 5. Similarly, if the vector polarizations or the scalar polarization is only considered, the corresponding distributions of inclination angle will be

$$\begin{aligned} p_{\text{vector}}(\iota) &\propto (\sin^2 \iota \cos^2 \iota + \sin^2 \iota)^{3/2} \sin \iota, \\ p_{\text{scalar}}(\iota) &\propto \sin^7 \iota. \end{aligned} \quad (37)$$

Their curves are shown in Fig. 5 upper plot by the orange and green curves, respectively. These distributions show the favored inclinations by the different polarizations, the most favored inclination by the tensor polarization is around $\iota = 0.55$, the distributions of ι have the peaks around $\pi/2 = 1.57$ for both vector and scalar polarizations.

With only considering the $+$ and \times polarizations from GR, the SNRs varying with the inclinations from two selected sources are shown in the lower plot of Fig. 5. The

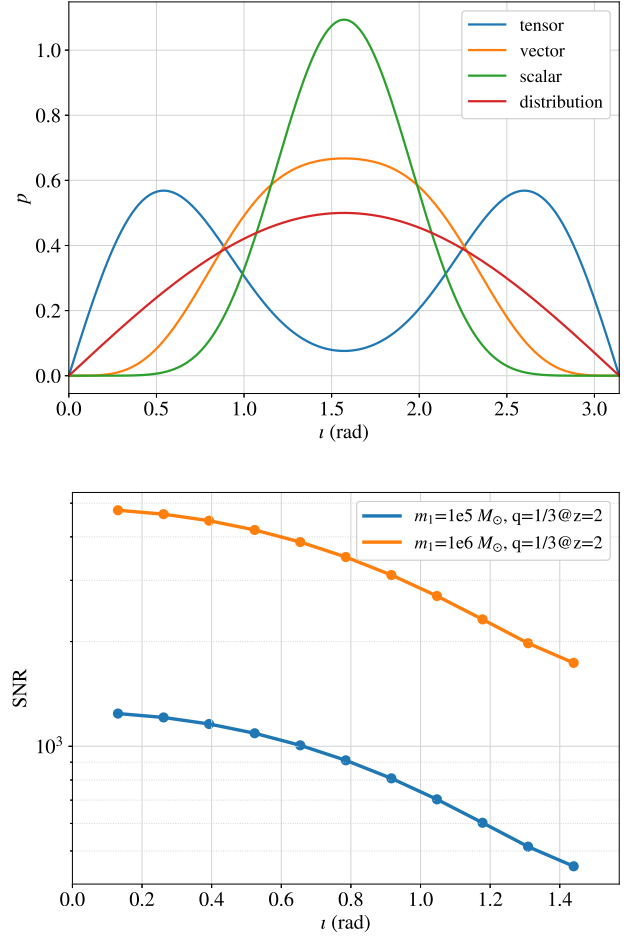


FIG. 5. The distributions of the inclination ι from expected detections considering the solo tensor, vector, and scalar polarization modes (upper panel) and the SNR of tensor polarizations from two selected sources with the inclinations (lower panel). The *tensor* curve shows the distribution of ι from the standard GR GW detections which described by Eq. (36) [51]. The *vector* and *scalar* curve show the distributions of ι when the solo vector or scalar polarization GW waveform is detected as described by Eq. 37. The *distribution* curve shows the distribution of ι from geometry, $p(\iota) \propto \sin \iota$.

SNR from $(\iota = \pi/2, \text{edge-on})$ will be $1/\sqrt{8}$ of SNR from $(\iota = 0/\pi, \text{face-on/off})$. For the inclination selection, considering the symmetry effects of the inclination in $[0, \pi/2]$ and $[\pi/2, \pi]$ range, we perform the investigations from $\iota = i\pi/24$ ($i = 1$ to 11). One reason to avoid the $\iota = 0$ is the astrophysical unlikely as shown in the upper plot of Fig. 5, another reason is that $\iota = 0$ or $\pi/2$ will dissolve some polarizations and make the FIM singular. And the ppE parameters are fixed for the FIM calculations which are $(b, \beta, \alpha_b, \alpha_L, \alpha_x, \alpha_y) = (-3, 0.01, 0, 0, 0, 0)$.

The constraints on ppE parameters from the source1 ($m_1 = 10^5 M_\odot, q = 1/3, z = 2$) observations for different inclination angles are shown in Fig. 6. The uncertainties of ppE parameters β and b get improved when

the inclination approaches 0 (or π) as shown in the two plots in the first row. Comparing to the LISA single detector, the joint LISA-TAIJI observation can improve the accuracy of the determination by a factor of ~ 2 which should be contribution of twofold SNR. When the position of sources are known and location parameters (λ, θ, D) are excluded, it only slightly improves the constraints from the single LISA observation, and dose not show improvement for the LISA-TAIJI joint observation. As the $\iota = 0.55$, the uncertainty of β measurement could be in 2.2×10^{-5} from LISA observation, and it could be constrained in 10^{-5} by the joint observation. The uncertainty of parameter b could be bound in 1.2×10^{-3} by LISA, and be within 6×10^{-4} by the LISA-TAIJI network.

The measurement uncertainties of ppE α_i from the source1 are shown by the middle and lower plots in Fig. 6. For these four parameters, the joint LISA-TAIJI network presents significant advantages. Without knowing the position of the source, the joint observation could improve the parameter measurements by more than ~ 10 times in most of the case, except the measurement on parameter α_x is improved by a factor of ~ 3 . For the α_b, α_L and α_y , their uncertainties tend to decrease with the increase of the selected ι list, and the α_x is better measured around the $\iota = \pi/4$. We infer these tendencies from Eq. (24) that the amplitudes of scalar breathing, scalar longitudinal, and vector y polarization modes increase with the selected inclination angles, and the amplitude of vector x mode has the maximum at $\iota = \pi/4$. When the inclination $\iota = 0.55$, the joint LISA-TAIJI observation could improve the parameter accuracy by more than 10 times compared to single LISA observation for α_b, α_L , and α_y ; if the position of the source is known and excluded from FIM calculation, the uncertainties of parameters could further decrease, and this should be due to the degeneracy between the distance and α_i is removed.

The constraints on ppE parameters from the source2 ($m_1 = 10^6 M_\odot, q = 1/3, z = 2$) observations for different inclination angles are shown in Fig. 7. Comparing the first two plots in Fig. 6 and 7, the source1 shows a better ability to measure parameters β and b than the source2. This could be due to the source1 has a relatively large frequency range in 30 days evolution, then has larger range of the u_2 . And this could improve parameter measurement [52]. The uncertainties of parameters α_b and α_L are slightly worse than the source1 as the two plots shown in the middle row. However, the measurement on the α_x and α_y are better than the results from source1. In general, at any inclination case, the joint LISA-TAIJI observation could improve the β and b determinations by a factor of ~ 2 , and improve the α_i determinations by a factor more than 10 in the optimistic scenario.

D. Results with varying ppE parameters b and β

In this subsection, we examine the impact of the joint LISA-TAIJI observation on the measurements of ppE parameters β and b with their different given values. As aforementioned, the inclination ι of a source tunes the amplitudes of each GW polarization and affects the SNR of the detection. By assuming the tensor polarization is dominant for the GW radiation from the coalescing compact binaries, we perform the investigations by choosing the fixed $\iota = 0.55$. The four α_i coefficient on polarization amplitudes are set to be zero as fiducial value ($\alpha_b = \alpha_L = \alpha_x = \alpha_y = 0$). Considering the parameter β has been bound at a given b from the PSR J0737-3039 [57] and the LIGO and LISA simulation [52], our choices of β at a given b are shown by the purple triangles in Fig. 8. And the FIM is calculated subsequently by settling each pair β and b .

The constraints on the parameters β and b are shown in Fig. 8. The upper two plots show the results from the source1 ($m_1 = 10^5 M_\odot, q = 1/3, z = 2$), and the lower two plots shows the results from source2 ($m_1 = 10^6 M_\odot, q = 1/3, z = 2$). As we can read from the left two plots, for the presets of β and b , the constraints on β get better with the b decreases for both two selected sources. The source1 shows relatively better determination on β by around one order than the source2 for the ($\beta = 10^{-2}, b = -3$). For other cases, no significant difference between their results. The joint observation of the LISA-TAIJI network could improve by a factor of ~ 2 as shown more clearly in the previous subsection. For the measurement on parameter b , the source1 demonstrates the more than 10 times better constraint than source2 for the $b < -4.5$. And the joint observation also can improve by a factor of 2 on the parameter determination. The knowledge of the source position has a marginal improvement on the measurement in most of the cases. The measurements of α_i values are relatively independent of the β and b selection and the results are not shown here.

As we can conclude that, for the ppE parameter ($\beta, b, \alpha_b, \alpha_L, \alpha_x, \alpha_y$) measurements, compared to the LISA single detector observation, the joint observation of the LISA and TAIJI network could improve for the β and b measurement by a factor of ~ 2 , the coefficients of alternative polarization modes, ($\alpha_b, \alpha_L, \alpha_y$), could be improved by ~ 10 times in any case. With knowing the position of the source, all the accuracy of polarization coefficients ($\alpha_b, \alpha_L, \alpha_x, \alpha_y$) could be improved by more than 10 times.

V. CONCLUSIONS

In this work, we explore the detectability of the LISA-TAIJI network to the alternative polarization modes compared to the single LISA mission. The ppE formulation is employed to specify the parameters ($\beta, b, \alpha_b, \alpha_L, \alpha_x, \alpha_y$) to be determined. To perform the in-

vestigations, two sources are selected which are source1 ($m_1 = 10^5 M_\odot, q = 1/3$) at redshift $z = 2$, and source2 ($m_1 = 10^6 M_\odot, q = 1/3$) at the same distance. By using the Fisher matrix algorithm, for the last 30 days to coalescence, the ppE parameters are generally better measured from the source1 observation than the source2.

The joint LISA-TAIJI network could improve the measurement of β and b by a factor of ~ 2 compared to the single LISA mission. The joint observations show the significant improvement for the uncertainty of the alternative polarization modes coefficients α_i , and the joint network could reduce the uncertainty of the α_b , α_L , and α_y by a factor of ≥ 10 compared to LISA. In an optimistic scenario, if the location of the source is determined by the multi-messenger observation, the joint LISA-TAIJI observation could further improve the measurement of four coefficients of alternative polarization modes α_i , which should be an outcome of the degeneracies between the source distance and coefficients are removed.

The current study employs the Fisher information matrix algorithm to determine the uncertainties of the ppE parameters with a single event, and only the approximate limits are achieved from this investigation. The Bayesian approaches have been proposed by Del Pozzo *et al.* [58] and Cornish *et al.* [52] to test the alternative gravitational

theories. And more rigorous bounds could be obtained by applying the Bayesian algorithm to the LISA-TAIJI joint observation. On the other side, the ppE parameters as the physical parameters should be consistent in all binary systems. The combined multiple detections are expected to put more stringent constraints on the values, and the method has been proposed by Del Pozzo *et al.* [59] to probe the neutron star equation of state with second-generation ground based detectors. We plan to perform these analyses in future studies.

ACKNOWLEDGMENTS

This work was supported by NSFC Nos. 12003059 and 11773059, Key Research Program of Frontier Sciences, Chinese Academy of Science, No. QYZDB-SSW-SYS016 and the Strategic Priority Research Program of the Chinese Academy of Sciences under grant Nos. XDA1502070102, XDA15020700 and XDB21010100. and by the National Key Research and Development Program of China under Grant Nos. 2016YFA0302002 and 2017YFC0601602. This work made use of the High Performance Computing Resource in the Core Facility for Advanced Research Computing at Shanghai Astronomical Observatory.

-
- [1] B. P. Abbott, R. Abbott, T. D. Abbott, S. Abraham, F. Acernese, K. Ackley, C. Adams, and et. al., Gwtc-1: A gravitational-wave transient catalog of compact binary mergers observed by ligo and virgo during the first and second observing runs, .
 - [2] R. Abbott, T. D. Abbott, S. Abraham, F. Acernese, K. Ackley, A. Adams, C. Adams, R. X. Adhikari, V. B. Adya, C. Affeldt, M. Agathos, K. Agatsuma, N. Aggarwal, O. D. Aguiar, L. Aiello, A. Ain, P. Ajith, S. Akcay, G. Allen, A. Allocca, P. A. Altin, A. Amato, S. Anand, A. Ananyeva, S. B. Anderson, W. G. Anderson, S. V. Angelova, S. Ansoldi, J. M. Antelis, S. Antier, S. Appert, K. Arai, M. C. Araya, J. S. Areeda, and et. al., .
 - [3] B. P. Abbott, R. Abbott, T. D. Abbott, M. R. Abernathy, F. Acernese, K. Ackley, C. Adams, T. Adams, P. Addesso, R. X. Adhikari, V. B. Adya, C. Affeldt, M. Agathos, K. Agatsuma, N. Aggarwal, O. D. Aguiar, L. Aiello, A. Ain, P. Ajith, B. Allen, A. Allocca, P. A. Altin, S. B. Anderson, W. G. Anderson, K. Arai, M. C. Araya, LIGO Scientific, and Virgo Collaborations, Tests of General Relativity with GW150914, *Phys. Rev. Lett.* **116**, 221101 (2016), arXiv:1602.03841 [gr-qc].
 - [4] B. P. Abbott, R. Abbott, T. D. Abbott, S. Abraham, F. Acernese, K. Ackley, C. Adams, R. X. Adhikari, V. B. Adya, C. Affeldt, M. Agathos, K. Agatsuma, N. Aggarwal, O. D. Aguiar, L. Aiello, A. Ain, P. Ajith, G. Allen, A. Allocca, M. A. Aloy, P. A. Altin, A. Amato, A. Ananyeva, S. B. Anderson, W. G. Anderson, S. V. Angelova, S. Antier, S. Appert, K. Arai, M. C. Araya, J. S. Areeda, M. Arène, N. Arnaud, K. G. Arun, S. Ascenzi, G. Ashton, S. M. Aston, P. Astone, F. Aubin, V. Avendano, A. Avila-Alvarez, S. Babak, P. Bacon, F. Badaracco, M. K. M. Bader, S. Bae, P. T. Baker, F. Baldaccini, G. Ballardin, S. W. Ballmer, S. Banagiri, J. C. Barayoga, S. E. Barclay, B. C. Barish, D. Barker, K. Barkett, LIGO Scientific Collaboration, and Virgo Collaboration, Tests of general relativity with the binary black hole signals from the LIGO-Virgo catalog GWTC-1, *Phys. Rev. D* **100**, 104036 (2019), arXiv:1903.04467 [gr-qc].
 - [5] The LIGO Scientific Collaboration, the Virgo Collaboration, R. Abbott, T. D. Abbott, S. Abraham, F. Acernese, K. Ackley, A. Adams, C. Adams, R. X. Adhikari, V. B. Adya, C. Affeldt, M. Agathos, K. Agatsuma, N. Aggarwal, O. D. Aguiar, L. Aiello, A. Ain, P. Ajith, G. Allen, A. Allocca, P. A. Altin, A. Amato, S. Anand, A. Ananyeva, S. B. Anderson, W. G. Anderson, S. V. Angelova, S. Ansoldi, J. M. Antelis, S. Antier, S. Appert, K. Arai, M. C. Araya, J. S. Areeda, M. Arène, N. Arnaud, S. M. Aronson, K. G. Arun, Y. Asali, S. Ascenzi, G. Ashton, S. M. Aston, P. Astone, F. Aubin, P. Aufmuth, K. AultONeal, C. Austin, V. Avendano, S. Babak, F. Badaracco, M. K. M. Bader, S. Bae, A. M. Baer, S. Bagnasco, J. Baird, M. Ball, G. Ballardin, S. W. Ballmer, A. Bals, A. Balsamo, G. Baltus, S. Banagiri, D. Bankar, R. S. Bankar, J. C. Barayoga, C. Barbiere, B. C. Barish, D. Barker, P. Barneo, S. Barnum, F. Barone, B. Barr, and et. al., Tests of General Relativity with Binary Black Holes from the second LIGO-Virgo Gravitational-Wave Transient Catalog, arXiv e-prints ,

- arXiv:2010.14529 (2020), arXiv:2010.14529 [gr-qc].
- [6] C. Brans and R. H. Dicke, Mach's Principle and a Relativistic Theory of Gravitation, *Physical Review* **124**, 925 (1961).
 - [7] C. M. Will, The Confrontation between General Relativity and Experiment, *Living Rev. Rel.* **17**, 4 (2014), arXiv:1403.7377 [gr-qc].
 - [8] T. Jacobson and D. Mattingly, Einstein-aether waves, *Phys. Rev. D* **70**, 024003 (2004), arXiv:gr-qc/0402005 [gr-qc].
 - [9] J. D. Bekenstein, Relativistic gravitation theory for the modified Newtonian dynamics paradigm, *Phys. Rev. D* **70**, 083509 (2004), arXiv:astro-ph/0403694 [astro-ph].
 - [10] N. Rosen, Theory of gravitation, *Phys. Rev. D* **3**, 2317 (1971).
 - [11] N. Rosen, A theory of gravitation, *Annals of Physics* **84**, 455 (1974).
 - [12] A. P. Lightman and D. L. Lee, New two-metric theory of gravity with prior geometry, *Phys. Rev. D* **8**, 3293 (1973).
 - [13] K. Chatziioannou, N. Yunes, and N. Cornish, Model-independent test of general relativity: An extended post-Einsteinian framework with complete polarization content, *Phys. Rev. D* **86**, 022004 (2012), arXiv:1204.2585 [gr-qc].
 - [14] B. P. Abbott, R. Abbott, T. D. Abbott, F. Acernese, K. Ackley, C. Adams, T. Adams, P. Addesso, R. X. Adhikari, V. B. Adya, C. Affeldt, M. Afrough, B. Agarwal, M. Agathos, K. Agatsuma, N. Aggarwal, O. D. Aguiar, L. Aiello, A. Ain, P. Ajith, B. Allen, G. Allen, A. Allocca, P. A. Altin, A. Amato, A. Ananyeva, S. B. Anderson, W. G. Anderson, S. V. Angelova, S. Antier, S. Appert, K. Arai, M. C. Araya, J. S. Areeda, N. Arnaud, K. G. Arun, S. Ascenzi, G. Ashton, M. Ast, S. M. Aston, P. Astone, D. V. Atallah, P. Aufmuth, and et. al. (LIGO Scientific Collaboration and Virgo Collaboration), Gw170814: A three-detector observation of gravitational waves from a binary black hole coalescence, *Phys. Rev. Lett.* **119**, 141101 (2017).
 - [15] H. Takeda, A. Nishizawa, Y. Michimura, K. Nagano, K. Komori, M. Ando, and K. Hayama, Polarization test of gravitational waves from compact binary coalescences, *Phys. Rev. D* **98**, 022008 (2018).
 - [16] H. Takeda, A. Nishizawa, K. Nagano, Y. Michimura, K. Komori, M. Ando, and K. Hayama, Prospects for gravitational-wave polarization tests from compact binary mergers with future ground-based detectors, *Phys. Rev. D* **100**, 042001 (2019).
 - [17] Y. Hagihara, N. Era, D. Iikawa, A. Nishizawa, and H. Asada, Constraining extra gravitational wave polarizations with advanced ligo, advanced virgo, and kagra and upper bounds from gw170817, *Phys. Rev. D* **100**, 064010 (2019).
 - [18] H. Takeda, S. Morisaki, and A. Nishizawa, Pure polarization test of GW170814 and GW170817 using waveforms consistent with modified theories of gravity, arXiv e-prints , arXiv:2010.14538 (2020), arXiv:2010.14538 [gr-qc].
 - [19] KAGRA Collaboration, T. Akutsu, M. Ando, and e. a. Arai, Overview of KAGRA : KAGRA science, arXiv e-prints , arXiv:2008.02921 (2020), arXiv:2008.02921 [gr-qc].
 - [20] P. Amaro-Seoane, H. Audley, S. Babak, and et al (LISA Team), Laser Interferometer Space Antenna, arXiv e-prints , arXiv:1702.00786 (2017).
 - [21] W.-R. Hu and Y.-L. Wu, The Taiji Program in Space for gravitational wave physics and the nature of gravity, *Natl. Sci. Rev.* **4**, 685 (2017).
 - [22] J. Luo *et al.* (TianQin Team), TianQin: a space-borne gravitational wave detector, *Class. Quant. Grav.* **33**, 035010 (2016), arXiv:1512.02076 [astro-ph.IM].
 - [23] W.-H. Ruan, C. Liu, Z.-K. Guo, Y.-L. Wu, and R.-G. Cai, The LISA-Taiji network, *Nature Astron.* **4**, 108 (2020), arXiv:2002.03603 [gr-qc].
 - [24] G. Wang, W.-T. Ni, W.-B. Han, S.-C. Yang, and X.-Y. Zhong, Numerical simulation of sky localization for LISA-TAIJI joint observation, *Phys. Rev. D* **102**, 024089 (2020), arXiv:2002.12628.
 - [25] H. Omiya and N. Seto, Searching for anomalous polarization modes of the stochastic gravitational wave background with LISA and Taiji, *Phys. Rev. D* **102**, 084053 (2020), arXiv:2010.00771 [gr-qc].
 - [26] G. Orlando, M. Pieroni, and A. Ricciardone, Measuring Parity Violation in the Stochastic Gravitational Wave Background with the LISA-Taiji network, (2020), arXiv:2011.07059 [astro-ph.CO].
 - [27] C. Liu, W.-H. Ruan, and Z.-K. Guo, Constraining gravitational-wave polarizations with Taiji, *Phys. Rev. D* **102**, 124050 (2020), arXiv:2006.04413 [gr-qc].
 - [28] P. C. Peters and J. Mathews, Gravitational Radiation from Point Masses in a Keplerian Orbit, *Physical Review* **131**, 435 (1963).
 - [29] P. C. Peters, Gravitational Radiation and the Motion of Two Point Masses, *Physical Review* **136**, 1224 (1964).
 - [30] S. Husa, Michele maggiore: Gravitational waves. volume 1: theory and experiments, *General Relativity and Gravitation* **41**, 1667 (2009).
 - [31] K. S. Thorne and C. M. Will, Theoretical Frameworks for Testing Relativistic Gravity. I. Foundations, *Astrophys. J.* **163**, 595 (1971).
 - [32] C. M. Will, Theoretical Frameworks for Testing Relativistic Gravity. 2. Parametrized Post-Newtonian Hydrodynamics, and the Nordtvedt Effect, *Astrophys. J.* **163**, 611 (1971).
 - [33] W.-T. Ni, Theoretical frameworks for testing relativistic gravity. iv. a compendium of metric theories of gravity and their post-newtonian limits, *Astrophys. J.* **176**, 769 (1972).
 - [34] N. Yunes and F. Pretorius, Fundamental theoretical bias in gravitational wave astrophysics and the parametrized post-Einsteinian framework, *Phys. Rev. D* **80**, 122003 (2009), arXiv:0909.3328 [gr-qc].
 - [35] G. Wang and W.-T. Ni, Numerical simulation of time delay interferometry for TAIJI and new LISA, *Res. Astron. Astrophys.* **19**, 058 (2019), arXiv:1707.09127 [astro-ph.IM].
 - [36] G. Wang, W.-T. Ni, W.-B. Han, and C.-F. Qiao, Algorithm for TDI numerical simulation and sensitivity investigation, (2020), arXiv:2010.15544 [gr-qc].
 - [37] M. Vallisneri and C. R. Galley, Non-sky-averaged sensitivity curves for space-based gravitational-wave observatories, *Class. Quant. Grav.* **29**, 124015 (2012), arXiv:1201.3684 [gr-qc].

- [38] M. Otto, G. Heinzel, and K. Danzmann, TDI and clock noise removal for the split interferometry configuration of LISA, *Class. Quant. Grav.* **29**, 205003 (2012).
- [39] M. Otto, Time-Delay Interferometry Simulations for the Laser Interferometer Space Antenna (2015).
- [40] M. Tinto and O. Hartwig, Time-Delay Interferometry and Clock-Noise Calibration, *Phys. Rev. D* **98**, 042003 (2018), arXiv:1807.02594 [gr-qc].
- [41] T. A. Prince, M. Tinto, S. L. Larson, and J. W. Armstrong, The LISA optimal sensitivity, *Phys. Rev. D* **66**, 122002 (2002), arXiv:gr-qc/0209039 [gr-qc].
- [42] M. Vallisneri, J. Crowder, and M. Tinto, Sensitivity and parameter-estimation precision for alternate LISA configurations, *Class. Quant. Grav.* **25**, 065005 (2008), arXiv:0710.4369 [gr-qc].
- [43] F. B. Estabrook and H. D. Wahlquist, Response of Doppler spacecraft tracking to gravitational radiation., *General Relativity and Gravitation* **6**, 439 (1975).
- [44] H. Wahlquist, The Doppler response to gravitational waves from a binary star source., *General Relativity and Gravitation* **19**, 1101 (1987).
- [45] K. Chatziioannou, N. Yunes, and N. Cornish, Model-Independent Test of General Relativity: An Extended post-Einsteinian Framework with Complete Polarization Content, *Phys. Rev. D* **86**, 022004 (2012), [Erratum: *Phys. Rev. D* **95**, 129901 (2017)], arXiv:1204.2585 [gr-qc].
- [46] S. Khan, S. Husa, M. Hannam, F. Ohme, M. Pürrer, X. J. Forteza, and A. Bohé, Frequency-domain gravitational waves from nonprecessing black-hole binaries. II. A phenomenological model for the advanced detector era, *Phys. Rev. D* **93**, 044007 (2016), arXiv:1508.07253 [gr-qc].
- [47] Z. Luo, Z. Guo, G. Jin, Y. Wu, and W. Hu, A brief analysis to Taiji: Science and technology, *Results in Physics* **16**, 102918 (2020).
- [48] G. Wang, W.-T. Ni, and W.-B. Han, Sensitivity investigation for unequal-arm LISA and TAIJI: the first-generation time-delay interferometry optimal channels, (2020), arXiv:2008.05812 [gr-qc].
- [49] M. Tinto and M. E. da Silva Alves, LISA Sensitivities to Gravitational Waves from Relativistic Metric Theories of Gravity, *Phys. Rev. D* **82**, 122003 (2010), arXiv:1010.1302 [gr-qc].
- [50] C. Zhang, Q. Gao, Y. Gong, D. Liang, A. J. Weinstein, and C. Zhang, Frequency response of time-delay interferometry for space-based gravitational wave antenna, *Phys. Rev. D* **100**, 064033 (2019), arXiv:1906.10901 [gr-qc].
- [51] B. F. Schutz, Networks of gravitational wave detectors and three figures of merit, *Class. Quant. Grav.* **28**, 125023 (2011), arXiv:1102.5421 [astro-ph.IM].
- [52] N. Cornish, L. Sampson, N. Yunes, and F. Pretorius, Gravitational Wave Tests of General Relativity with the Parameterized Post-Einsteinian Framework, *Phys. Rev. D* **84**, 062003 (2011), arXiv:1105.2088 [gr-qc].
- [53] C. Cutler and É. E. Flanagan, Gravitational waves from merging compact binaries: How accurately can one extract the binary's parameters from the inspiral waveform?, *Phys. Rev. D* **49**, 2658 (1994), arXiv:gr-qc/9402014 [gr-qc].
- [54] C. Cutler, Angular resolution of the LISA gravitational wave detector, *Phys. Rev. D* **57**, 7089 (1998), arXiv:gr-qc/9703068 [gr-qc].
- [55] M. Vallisneri, Use and abuse of the Fisher information matrix in the assessment of gravitational-wave parameter-estimation prospects, *Phys. Rev. D* **77**, 042001 (2008), arXiv:gr-qc/0703086 [GR-QC].
- [56] K. A. Kuns, H. Yu, Y. Chen, and R. X. Adhikari, Astrophysics and cosmology with a decihertz gravitational-wave detector: TianGO, (2019), arXiv:1908.06004 [gr-qc].
- [57] N. Yunes and S. A. Hughes, Binary Pulsar Constraints on the Parameterized post-Einsteinian Framework, *Phys. Rev. D* **82**, 082002 (2010), arXiv:1007.1995 [gr-qc].
- [58] W. Del Pozzo, J. Veitch, and A. Vecchio, Testing General Relativity using Bayesian model selection: Applications to observations of gravitational waves from compact binary systems, *Phys. Rev. D* **83**, 082002 (2011), arXiv:1101.1391 [gr-qc].
- [59] W. Del Pozzo, T. G. F. Li, M. Agathos, C. Van Den Broeck, and S. Vitale, Demonstrating the feasibility of probing the neutron star equation of state with second-generation gravitational wave detectors, *Phys. Rev. Lett.* **111**, 071101 (2013), arXiv:1307.8338 [gr-qc].

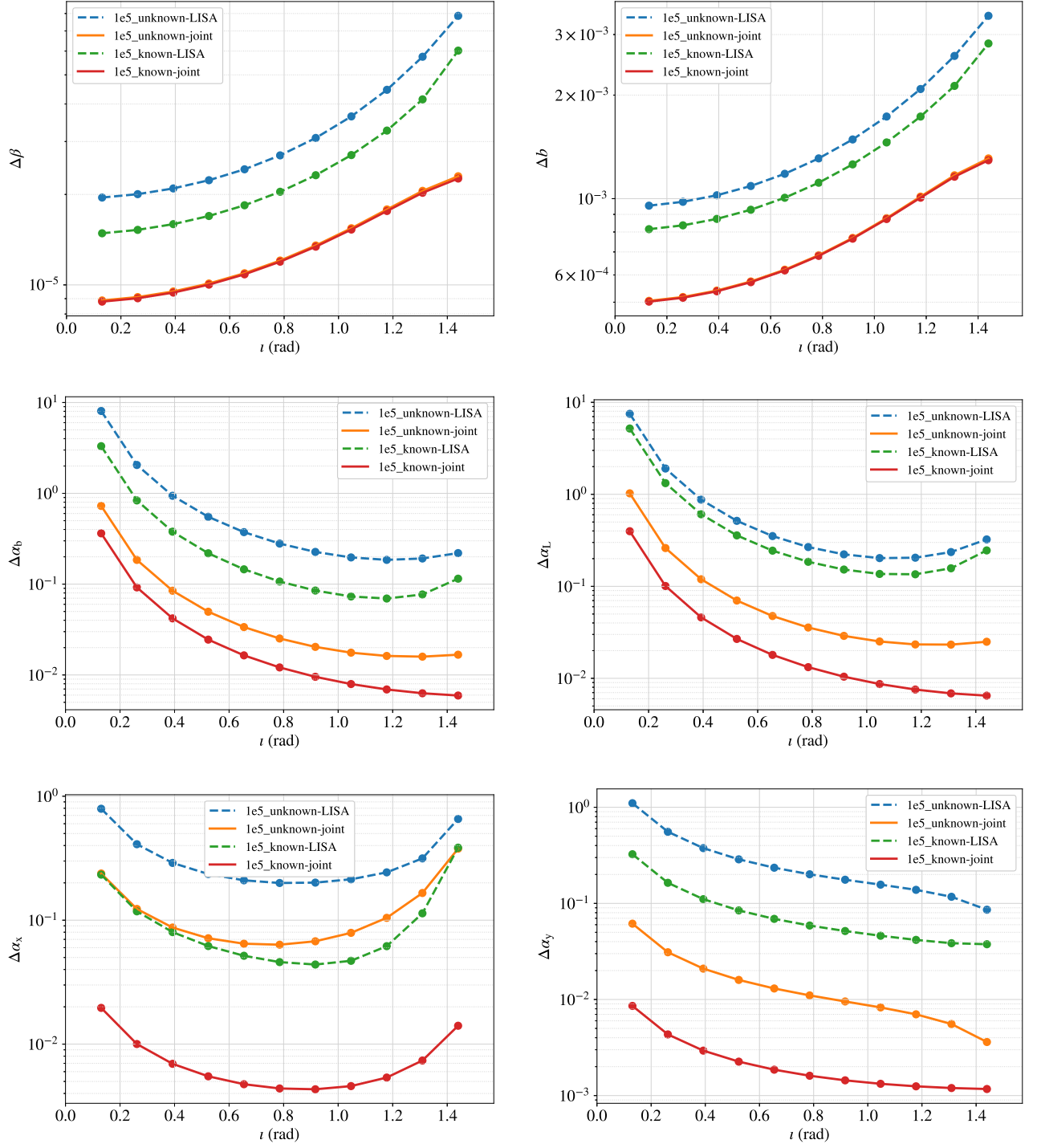


FIG. 6. The uncertainties of ppE parameters varying with the inclination ι from the source1 ($m_1 = 10^5 M_\odot, q = 1/3, z = 2$) for ppE parameters setup $(\beta, b, \alpha_b, \alpha_L, \alpha_x, \alpha_y) = (0.01, -3, 0, 0, 0, 0)$. Four scenarios results are shown in each plots which are, 1) the result from the single LISA observation without knowing the source location (1e5_unknown-LISA), 2) the result from joint LISA-TAIJI observation without information of source position (1e5_unknown-joint), 3) the result from the LISA observation with knowing position of the source and the FIM excluding the three position parameters: direction of the source (λ, θ), and distance of the source D (1e5_known-LISA), and 4) the result from LISA-TAIJI joint observation with knowing the position of the source (1e5_known-joint).

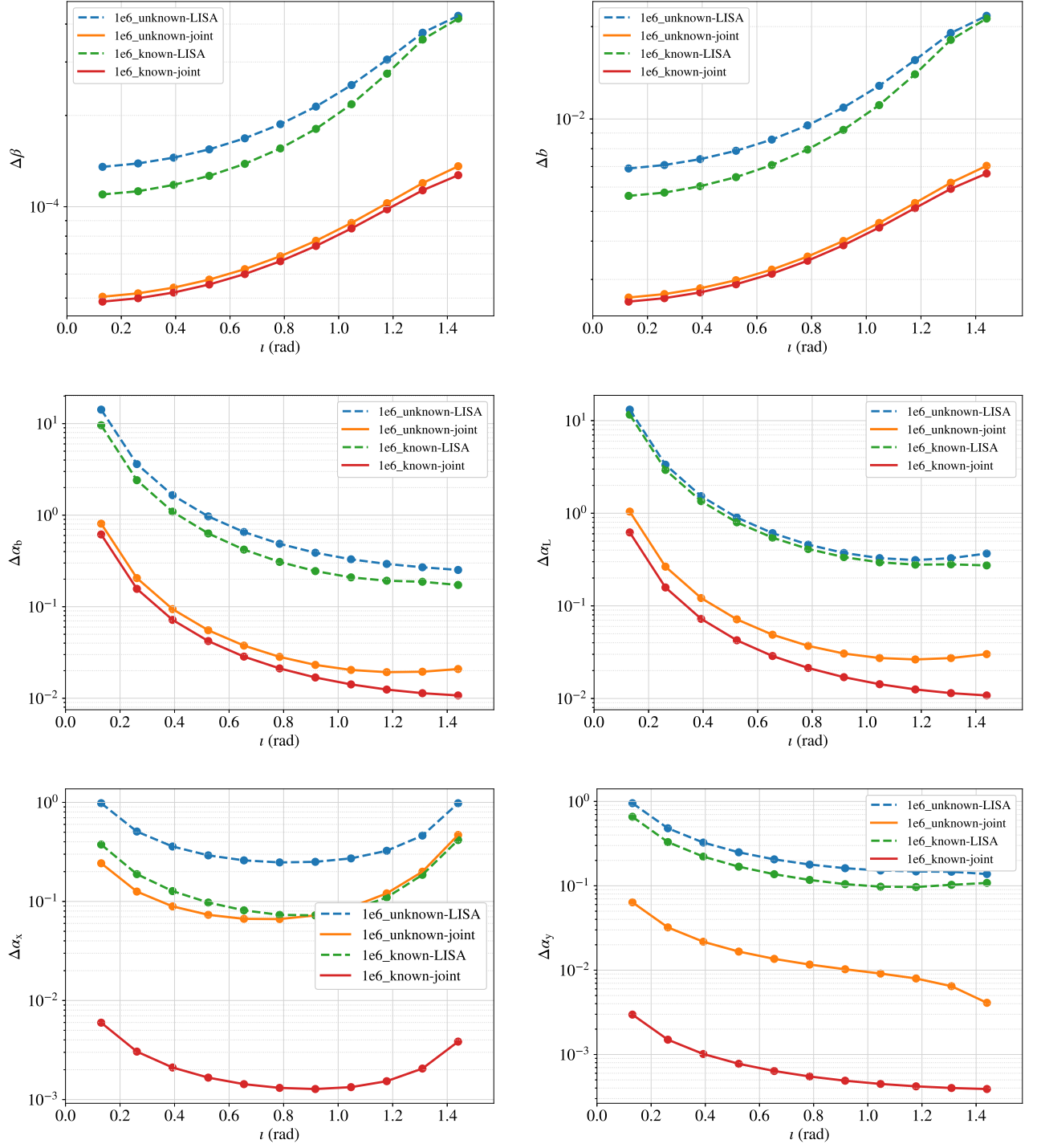


FIG. 7. The uncertainties of ppE parameters varying with the inclination ι from the source2 ($m_1 = 10^6 M_\odot, q = 1/3, z = 2$ for ppE parameters setup $(\beta, b, \alpha_b, \alpha_L, \alpha_x, \alpha_y) = (0.01, -3, 0, 0, 0, 0)$). Four scenarios results are shown in each plots which are 1) the result from the single LISA observation without knowing the position of the source (1e6_unknown-LISA), 2) the result from joint LISA-TAIJI observation without information of source location (1e6_unknown-joint), 3) the result from the LISA observation with knowing position of the source and the FIM calculation excluding the three parameters: direction of the source (λ, θ), and distance of the sources D (1e6_known-LISA), and 4) the result from LISA-TAIJI joint observation with knowing the position of the source (1e6_known-joint).

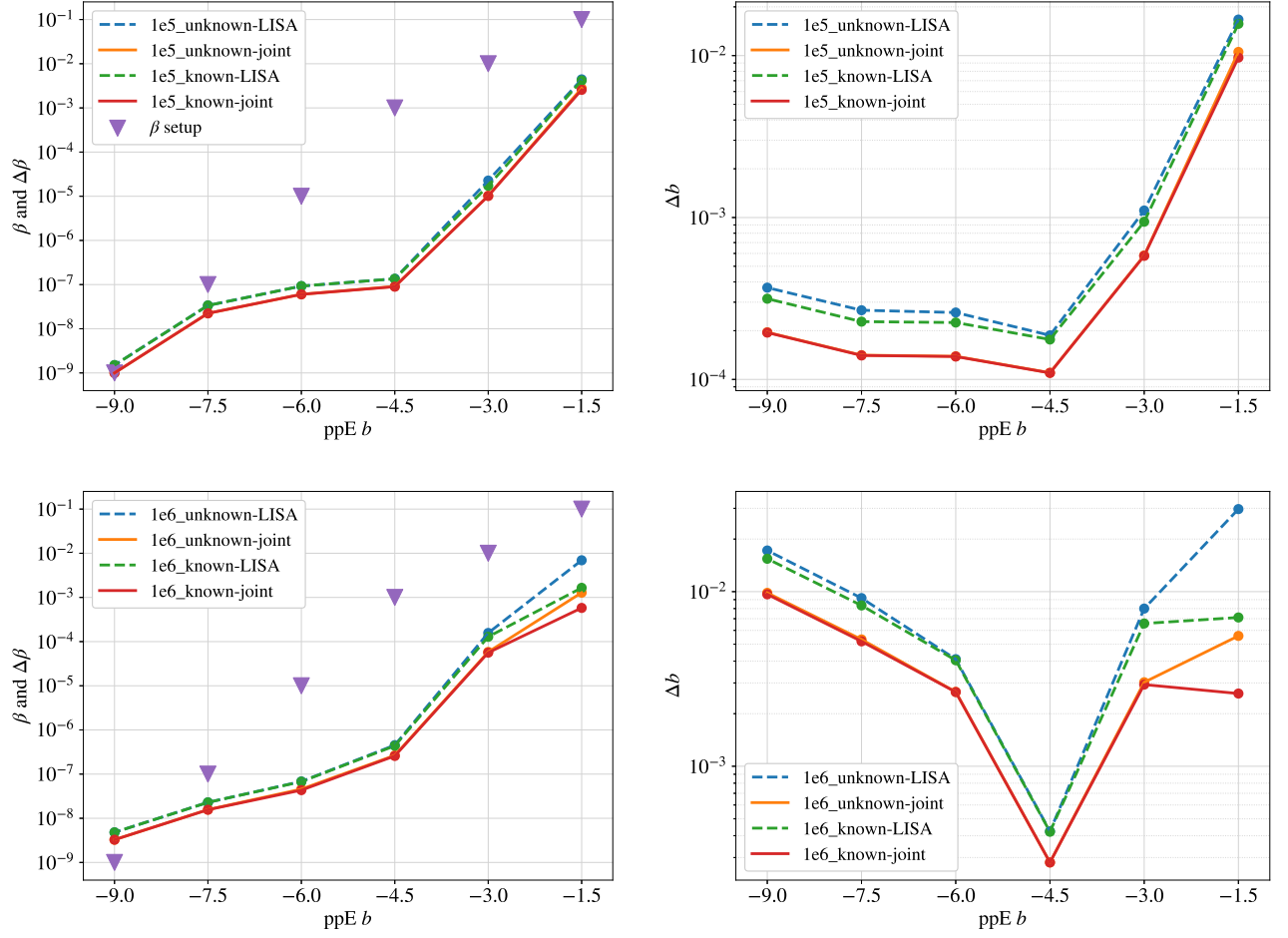


FIG. 8. The constraints of ppE parameter β and b from the LISA observation and LISA-TAIJI joint observations. The upper two plots show the results from the source1 ($m_1 = 10^5 M_\odot, q = 1/3, z = 2$), and the lower plots are the results from the source2 ($m_1 = 10^6 M_\odot, q = 1/3, z = 2$). The (purple) triangles are the β setups at a given b values which roughly referred from bounds in Cornish *et al.* [52]. The legend labels are same defined as in Fig. 6 and Fig. 7. The keyword with $1e5$ or $1e6$ indicates the respective source1 or source2, and a label with unknown/know shows if the position of source (λ, θ, D) is included/excluded in the FIM calculations.